
Article:
Kouanga, C.T., Jones, J.D., Revill, I. et al. (5 more authors) (2018) On the estimation of finite lifetime under fretting fatigue loading. International Journal of Fatigue, 112. pp. 138-152. ISSN 0142-1123

https://doi.org/10.1016/j.ijfatigue.2018.03.013

On the estimation of finite lifetime under fretting fatigue loading

C. T. Kouanga[1], J. D. Jones[2], I. Revill[3], A. Wormald[3], D. Nowell[4], R. S. Dwyer-Joyce[5], J. A. Araújo[6] and L. Susmel[1]

[1]Department of Civil and Structural Engineering, the University of Sheffield, Sheffield S1 3JD, UK
[2]Cummins Inc., Box 3005 M/C 50020, Columbus, IN 47202-3005, USA
[3]Cummins Daventry Technical Centre, Royal Oak Way South, Daventry, NN11 8NU, UK
[4]Department of Mechanical Engineering, Imperial College London, Kensington, London SW7 2AZ
[5]Department of Mechanical Engineering, the University of Sheffield, Sheffield S1 3JD, UK
[6]Department of Mechanical Engineering, University of Brasilia, 70910-900 Brasilia, DF, Brazil

Corresponding Author: Prof. **Luca Susmel**
Department of Civil and Structural Engineering
The University of Sheffield, Mappin Street, Sheffield, S1 3JD, UK
Telephone: +44 (0) 114 222 5073
Fax: +44 (0) 114 222 5700
e-mail: l.susmel@sheffield.ac.uk

ABSTRACT

The aim of this paper is to formulate and validate an alternative design approach suitable for predicting finite lifetime of mechanical assemblies subjected to constant amplitude (CA) fretting fatigue loading. The design methodology being proposed is based on the use of the Modified Wöhler Curve Method (MWCM) applied in conjunction with both the Theory of Critical Distance (TCD) and the Shear Stress-Maximum Variance Method (τ-MVM). In more detail, the TCD, applied in the form of the Point Method (PM), is used to take into account the damaging effect of the multiaxial stress gradients acting on the material in the vicinity of the contact region. The time-variable linear-elastic stress state at the critical locations is then post-processed according to the MWCM which is a bi-parametrical criterion that estimates fatigue lifetime via the stress components relative to those planes experiencing the maximum shear stress amplitude. Thanks to its specific features, the MWCM is capable of modelling not only the presence of non-zero mean stresses, but also the degree of multiaxiality and non-proportionality of the local load history being investigated. In this setting, the τ-MVM is used to calculate the stress quantities relative to the critical plane whose orientation is determined numerically by locating that plane containing the direction experiencing the maximum variance of the resolved shear stress. The accuracy and reliability of the proposed design methodology was checked against a number of experimental data taken from the literature and generated by testing four different metallic materials. The agreement between experiments and estimates being obtained strongly supports the idea that the proposed approach can be used to perform a rapid assessment of mechanical assemblies damaged by in-service fretting fatigue loading.

Keywords: Fretting fatigue, Fatigue life estimation, Theory of critical distances, Multiaxial fatigue

Nomenclature

a	Contact semi-width.
A, B	Material fatigue constants in the L_M vs. N_f relationship
E	Young's modulus
f	Friction coefficient
$F_{i,j,k}(t)$	External time-variable forces
k	Negative inverse slope of the fully-reversed uniaxial fatigue curve
k_0	Negative inverse slope of the fully-reversed torsional fatigue curve
$k_\tau(\rho_{eff})$	Negative inverse slope of the modified Wöhler curve
K_f	Notch fatigue strength reduction factor
K_t	Stress concentration factor referred the net area
L_M	Critical distance in the finite life regime
m	Mean stress sensitivity index
N_A	Reference number of cycles to failure
N_f	Experimental number of cycles to failure
$N_{f,e}$	Estimated number of cycles to failure
N_S	Reference number of cycles to failure in the low-cycle fatigue regime
P	Normal load
P_0	Peak pressure
Q	Shear load
Q_{max}	Amplitude of the shear load
r	Linear coordinate associated with the focus path
r_n	Notch root radius
R	Stress ratio
R_p	Pad radius
t	Time instant
ΔQ	Range of the shear force
$\Delta\sigma_1$	Range of the linear-elastic maximum principal stress
$\Delta\sigma_b$	Range of the bulk stress
ν	Poisson's ratio
ρ_{eff}	Effective critical plane stress ratio
ρ_{lim}	Intrinsic fatigue strength threshold
σ_A	Fully-reversed uniaxial endurance limit at N_A cycles to failure
σ_{An}	Fully-reversed uniaxial notch endurance limit
$\sigma_b(t)$	Bulk stress at a generic instant, t
$\sigma_{b,a}$	Amplitude of the bulk stress
$\sigma_{n,a}$	Amplitude of the stress perpendicular to the critical plane
$\sigma_{n,m}$	Mean stress perpendicular to the critical plane
$\sigma_{n,max}$	Maximum value of the stress perpendicular to the critical plane
$\sigma_{n,min}$	Maximum value of the stress perpendicular to the critical plane
σ_y	Yield stress
σ_{UTS}	Ultimate tensile strength
σ_S	Reference normal stress at N_S cycles to failure
$\tau(t)$	Time-variable shear stress
τ_a	Shear stress amplitude on the plane of maximum shear stress amplitude
τ_A	Fully-reversed torsional endurance limit at N_A cycles to failure
$\tau_{A,Ref}(\rho_{eff})$	Fatigue strength corresponding to N_{Ref} cycles
$\tau_{MV}(t)$	Resolved shear stress
$\tau_{MV,max}$	Maximum value of the resolved shear stress
$\tau_{MV,min}$	Minimum value of the resolved shear stress
τ_S	Reference shear stress at N_S cycles to failure

1. Introduction

Fretting is a damage mechanism that occurs at the surface of two contacting mechanical components. This type of damage results from a small amplitude oscillatory movement in the contact region. In particular, in those situations where one or both contacting components undergo cyclic loading, the damage resulting from fretting becomes more detrimental and is called “fretting fatigue” (Fig. 1). It is found that fretting reduces the lifetime of engineering materials, compared to plain fatigue [1]. Fretting fatigue damage is a particular issue in mechanical assemblies such as aircraft structural lap joints, dovetail blade/disk type attachments in gas turbine engines and at the contact interface between the cylinder block, head gasket and cylinder head of internal combustion engines. A number of physical, environmental and mechanical factors influence the initiation and propagation of fretting fatigue cracks. These include: contact geometry, contact load, coefficient of friction, bulk stress amplitude, material mechanical/fatigue properties, aggressiveness of the environment, and temperature [2].

Due to the complex nature of this structural/design problem and its significance in engineering applications of practical interest, extensive theoretical and experimental work has been carried out over the last 50 years. In this context, the problem of standardising fretting fatigue tests has been investigated since the late 80s [3, 4] and some of these testing protocols have been used successfully in different testing configurations, for instance, grip-type loading [5], single-clamp loading [6], and bridge-type loading [7].

Examination of the state of the art demonstrates that many approaches have been proposed (and validated) to predict crack initiation and propagation in assemblies subjected to constant amplitude (CA) loading. For example, Hojjati-Talemi et al. [8] used continuum damage mechanics to predict crack initiation lifetime under fretting fatigue conditions. Alternatively, Lykins et al. [9] attempted to model the fretting fatigue crack initiation process by using damage parameters such as those proposed by Fatemi & Socie [10], by Smith, Watson and Topper [11, 12], and by Ruiz [13]. Navarro et al. [14] estimated the total fretting fatigue lifetime of Al 7075-T6 specimens by considering both the crack initiation and the crack propagation phase. They suggested using a bespoke multiaxial crack initiation criterion that can be applied by directly post-processing the stress distribution in the vicinity of the contact region. To model the crack propagation part of the total lifetime, they

employed different fatigue crack growth laws which effectively modelled the initial short crack growth phase.

Nowell et al. [15] applied the critical distance concept [16] and a short crack arrest criterion [17] to predict fretting fatigue thresholds. The short crack arrest methodology was used to assess fretting fatigue damage for those contact configurations resulting in severe stress gradients. To validate their predictions, they used both the Hertzian fretting test results that were generated by Nowell himself [18] and the fretting fatigue experiments reported in Ref. [17] and carried out using 'flat and rounded' contact pads made of Ti-6A1-4V. They concluded that both criteria returned sound predictions and could be used to assess a wide range of applications including surface treated components. Nowell et al. [19] also investigated the fretting fatigue performance of blade-to-disc assemblies in aircraft gas turbines. In particular, they carried out a number of bespoke fatigue experiments to simulate the loading experienced by dovetail blade roots in turbines of aero-engines. To predict the fretting fatigue performance of their blade-type specimens, they suggested to use short crack arrest methods [17, 20] to post-process the stress fields obtained from conventional linear-elastic FE models.

Following a different philosophy to estimate the crack initiation lifetime of Al2024-T3 specimens subjected to CA fretting fatigue loading, Hojjati-Talemi et al. [21] used an uncoupled damage-evolution model based on a thermodynamic potential function, where the assumption was formed that the state of stress is not influenced by extent and evolution of damage. Recently, Noraphaiphipaksa et al. [22] carried out experiments and FE analyses to investigate the influence of cylindrical-on-flat and flat-on-flat contacts on the fretting fatigue behaviour of medium-carbon steel JIS S45C. They proposed use of the maximum shear stress range criterion [23] to predict the location of the crack nucleation sites and the maximum tangential stress range criterion [24] to estimate the orientation of fretting fatigue crack paths. Fretting fatigue life was estimated by integrating the fatigue crack growth curve from an initial to a critical crack length. They concluded that the predicted fretting fatigue lives were slightly shorter than the experimental ones. Finally, in a series of investigations, Araújo et al. [25-27] proposed to use the Modified Wöhler Curve Method (MWCM) along with the Theory of Critical Distance (TCD) [28, 29] to estimate fretting fatigue damage both in the high- and in the medium-cycle fatigue regime. As to the way this design methodology was implemented in its latest reformulation, it is worth observing that in Ref. [25] Araújo et al. used the

Maximum Rectangular Hull concept [30-33] to calculate the shear stress components relative to the critical plane that are needed to estimate fatigue damage according to the MWCM.

This paper presents a formal design methodology of general validity for estimating the life of mechanical assemblies under CA fretting fatigue loading. Following the approach of [25], damage is assessed according to the "notch analogue" concept [34] by post-processing the linear-elastic stress fields present near the trailing edge of the contact. More specifically, the proposed approach starts by assuming that the damage mechanisms in a metallic material subject fretting fatigue are similar to those observed in conventional notched components made of the same material and subjected to a cyclic load history [26].

To estimate the life of notched metals, Susmel et al. [35] reformulated the TCD to apply it also in the medium-cycle fatigue regime. This reformulation was based on the idea that the characteristic material length, L, increases as the number of cycle to failure, N_f, decreases. This assumption took as its starting point the experimental evidence that in metallic materials containing stress raisers the size of the plastic zone increases as the magnitude of the applied loading increases. This approach was validated by an extensive experimental investigation involving uniaxially loaded notched specimens made of cold-rolled low-carbon steel EN3B. Susmel et al. [36-40] have also argued that the life of notched components subjected to multiaxial loading paths can be predicted successfully by applying the MWCM in conjunction with the TCD, with the latter being used in the Point Method (PM) form. To validate this approach, they carried out experiments on cylindrical V-notched specimens of EN3B carbon steel. The specimens were subjected to in-phase and 90° out-of-phase tension and torsion loading with and without superimposed static stresses [36]. The authors concluded that the use of the MWCM along with the TCD was successful in predicting the fatigue lifetime of the notched steel.

Due to the similarities between notch fatigue and fretting fatigue [34], a design procedure based on the combined use of the MWCM, the TCD, and the Shear Stress-Maximum Variance Method (τ-MVM) is formalised in the present paper to allow a rapid estimation of finite lifetime of components subjected to CA fretting fatigue. The novelty in this method is that the τ-MVM [41] is employed to calculate the critical plane stresses that are needed to assess fretting fatigue damage according to the MWCM applied along with the PM.

2. The MWCM applied in conjunction with the TCD

The MWCM [28, 42, 43] is a medium/high-cycle multiaxial fatigue criterion that estimates fatigue life as a function of the stress components relative to the material plane experiencing the maximum shear stress amplitude (the so-called critical plane) [44, 45]. The formulation of the MWCM is based on the effective critical plane stress ratio, ρ_{eff}, which is defined as [46]:

$$\rho_{eff} = \frac{m \cdot \sigma_{n,m}}{\tau_a} + \frac{\sigma_{n,a}}{\tau_a} \quad (1)$$

In definition (1) $\sigma_{n,m}$, $\sigma_{n,a}$, τ_a are respectively the mean normal stress, the normal stress amplitude and the maximum shear stress amplitude relative to the critical plane. According to Kaufmann and Topper's model [47], material property m is a mean stress sensitivity index which ranges between 0 and 1. When m equals zero, the considered material is assumed to be insensitive to superimposed static stresses. In contrast, when m equals unity, the assessed material is fully sensitive to the presence of non-zero mean stresses [28, 46]. Further, according to the way ρ_{eff} is defined, this stress ratio models not only the presence of superimposed static stresses, but also the degree of multiaxiality and non-proportionality of the applied loading path [46].

The way the MWCM works is illustrated schematically using the log-log modified Wöhler diagram of Fig. 2 that plots the shear stress amplitude on to the critical plane, τ_a, against the number of cycle to failure, N_f. With this presentation, any modified Wöhler curve is defined via its slope, $-1/k_\tau(\rho_{eff})$, and the reference shear stress amplitude, $\tau_{A,Ref}(\rho_{eff})$, at a given number of cycles to failure, N_A. It is worth recalling here that $\rho_{eff} = 1$ is the fully-reversed uniaxial fatigue curve, whereas $\rho_{eff} = 0$ is the torsional fatigue curve [28]. As shown schematically in Fig. 2, experimental evidence demonstrates that, for conventional engineering metals, the modified Wöhler curves move downward in the diagram as ρ_{eff} increases [28, 48, 49]. In other words, for a given amplitude of shear stress on the critical plane, the extent of fatigue damage increases with stress ratio ρ_{eff} .

Recent investigations demonstrate that the functions $k_\tau(\rho_{eff})$ and $\tau_{A,Ref}(\rho_{eff})$ can be expressed effectively by linear equations, i.e. [36, 38]:

$$k_\tau(\rho_{eff}) = (k - k_0).\rho_{eff} + k_0 \qquad \text{for } \rho_{eff} \le \rho_{lim} \tag{2}$$

$$\tau_{A,Ref}(\rho_{eff}) = \left(\frac{\sigma_A}{2} - \tau_A\right) \cdot \rho_{eff} + \tau_A \quad \text{for } \rho_{eff} \le \rho_{lim} \tag{3}$$

where k and σ_A are the negative inverse slope and the endurance limit (extrapolated at N_A cycles to failure) characterising the fully-reversed uniaxial fatigue curve, whereas k_0 and τ_A are the corresponding quantities associated with the torsional fatigue curve. In Eqs (2) and (3) ρ_{lim} is an intrinsic fatigue strength threshold [50]. In more detail, the use of the MWCM under large values of stress ratio ρ_{eff} gives conservative estimates since when the mean stress perpendicular to the critical plane reaches a certain material-dependant threshold value, a further increase of $\sigma_{n,m}$ does not lead to additional fatigue damage [46, 50]. This can be explained by observing that, once the mean stress normal to the critical plane is larger than a threshold, micro/meso cracks are fully open and therefore the shear forces driving the Mode II propagation are fully transmitted to the crack tips rather than being partially supported by crack face friction [46, 47]. Hence, for $\rho_{eff} > \rho_{lim}$, the MWCM can still be applied by keeping the slope and reference point constant [51], i.e.:

$$k_\tau(\rho_{eff}) = (k - k_0).\rho_{lim} + k_0 \qquad \text{for } \rho_{eff} > \rho_{lim} \tag{4}$$

$$\tau_{A,Ref}(\rho_{eff}) = \left(\frac{\sigma_A}{2} - \tau_A\right) \cdot \rho_{lim} + \tau_A \quad \text{for } \rho_{eff} > \rho_{lim} \tag{5}$$

where

$$\rho_{lim} = \frac{\tau_A}{2\tau_A - \sigma_A} \tag{6}$$

In definition (6) σ_A and τ_A are the amplitudes of the fully-reversed plain endurance limit extrapolated at N_A cycles to failure under uniaxial and torsional fully-reversed fatigue loading, respectively. It is useful to recall here also that, as demonstrated in Ref. [48], Eq. (6) can be derived directly from Eq. (3) by simply re-writing the MWCM in terms of shear stress amplitude and maximum stress normal to the critical plane. In particular, the assumption can be made that the intrinsic mathematical limit that can be determined by reformulating our criterion in terms of τ_a and $\sigma_{n,max}$ corresponds to a

change in the physical mechanisms resulting in the initiation of fatigue cracks [28]. Therefore, Eq. (6) represents a material threshold above which the critical plane concept can be applied provided that it is modified to take into account the role of large values of the stresses perpendicular to the critical plane [46].

Turning back to the fatigue assessment problem, after determining the required modified Wöhler curve from Eqs (2) to (6), the number of cycle to failure can be predicted directly as follows [28]:

$$N_{f,e} = N_A \cdot \left[\frac{\tau_{A,ref}(\rho_{eff})}{\tau_a}\right]^{k_\tau(\rho_{eff})} \tag{7}$$

where ρ_{eff} and τ_a are values on the critical plane associated with the specific load history being investigated.

To estimate finite lifetime of notched components, the MWCM can be used in conjunction with the TCD applied in the form of the PM [36, 52]. This approach takes as its starting point the idea that the multiaxial stress gradients in the vicinity of the crack initiation location are modelled effectively by the TCD. In parallel, the MWCM is used to account for the presence of non-zero mean stresses as well as the degree of multiaxiality and non-proportionality of the local stress history under investigation [28, 35].

The TCD formalised in the form of PM was proposed by Peterson [53] in the middle of the last century. In particular, he argued that, as far as stress concentation phenomena are concerned, the linear-elastic reference stress to be compared to the plain fatigue limit of the material, σ_A, can be determined directly at a given distance from the tip of the notch being designed. A few decades later, Peterson's intuition was further developed by Tanaka [54] and by Taylor [29] who proposed a simple way of determining the required critical distance by combining the long crack threshold value of the stress intensity factor range with the plain fatigue limit. At the beginning of the current century, the accuracy obtained by using the PM to estimate high-cycle fatigue strength of notched components prompted a further development to make the TCD suitable for assessing notched components in the finite lifetime regime [35]. The extension is based on the observation that, in the medium-cycle fatigue regime, the critical distance, L_M, decreases as the number of cycles to failure, N_f, increases.

This trend can be explained by observing that, in the vicinity of the notch tip, the size of the plastic region increases as the magnitude of the applied cyclic loading increases. The TCD as employed in the present investigation is based on the assumption that the mechanical behaviour of engineering materials can be modelled effectively by simply using a linear-elastic constitutive law. Therefore, the fact that the size of the plastic zone increases as the magnitude of the cyclic loading decreases is captured by the linear-elastic TCD by making the critical length increase as the number of cycles to failure decreases [28, 35]. This behaviour can be modelled by using a simple power, i.e. [28, 35]:

$$L_M = A \cdot N_f^B \tag{8}$$

In Eq. (8) A and B are material constants to be determined from the un-notched fatigue curve together with a fatigue curve for specimens containing a known geometrical feature [35, 36]. Fig. 3 summarises the strategy that is recommended to be followed to determine fatigue constants A and B. In more detail, using the PM argument, the distance from the notch tip, $L_M/2$, at which the linear elastic maximum principal stress equals the stress which breaks the plain material at $N_f = N_{f,i}$ cycles to failure can be calculated using either analytical methods or FE models. The critical distance can then be estimated for any number of cycles to failure, allowing constants A and B to be determined. It is important to point out here also that, according to the key features of the TCD, the L_M vs. N_f relationship is a fatigue property that is different for different materials [35]. Further, given a material, the values of constants A and B are seen not to be affected markedly by the sharpness/profile of the notch being used for their calibration [28].

The procedure for using the MWCM in conjunction with the PM to estimate fatigue lifetime is summarised in Fig. 4. The first step is to determine the linear-elastic stress distribution along the focus path, i.e. the straight line normal to the free surface that emanates from the assumed crack initiation location (point A in Fig. 4a). The next step is to calculate the maximum shear stress amplitude, τ_a, and the associated value of the critical plane stress ratio, ρ_{eff}, along the above focus path (Fig. 4b). At any distance r from the assumed crack initiation point, A, given the corresponding values for τ_a and ρ_{eff}, the resulting Modified Wöhler curve can be estimated from the MWCM's governing equations (2) to (6) – see Figs 4c and 4d. Hence, the number of cycles to failure, N_f, can

be estimated at any point along the focus path (Fig. 4d) and then used together with Eq. (8) to calculate, for any value of r, the associated critical distance value, L_M. Finally, the notched component being assessed is assumed to fail at the number of cycles to failure, N_f, where the value of r matches the required critical distance from Eq. (8) (Fig. 4e) [28, 36], i.e.:

$$\frac{L_M(N_{f,e})}{2} = r \tag{9}$$

In practice, a simple recursive procedure is employed to vary r, as schematically shown in Fig. 4.

3. The Maximum Variance concept to determine the stress quantities relative to the critical plane under CA loading.

In order to apply the MWCM to estimate multiaxial fatigue lifetime of mechanical components, one of the most complex tasks is certainly the determination of the stress quantities relative to the critical plane, i.e. $\sigma_{n,m,}$ $\sigma_{n,a}$, and τ_a. In the present investigation it is proposed that fretting fatigue damage can be assessed by defining the required critical plane stress quantities according to the Shear Stress-Maximum Variance Method (τ-MVM) [43]. This approach defines the critical plane as that containing the direction which experiences the maximum variance of the resolved shear stress, $\tau_{MV}(t)$ [41, 43]. An algorithm which can be used to implement this approach was developed by Susmel [55]. The method has the advantage that, as soon as the variance and co-variance terms characterising the time-variable stress components of the stress tensor at the critical location are known [55], the computational time required to determine the orientation of the critical plane does not depend on the length of the assessed input load history. In particular, to use the conventional definitions to determine the critical plane, the load history under investigation must be projected on a large number of planes so that those experiencing the maximum shear stress amplitude can be identified [55]. In other words, according to this *modus operandi*, the load history being assessed must be post-processed a number of times equal to the number of material planes being explored to determine the critical one. In contrast, to identify the potential critical planes according to the τ-MVM, the load history being assessed is post-processed two times: one iteration is required to

determine the mean values of the stress components and a second iteration is needed to determine the variance and co-variance terms associated with the time-variable stress tensor at the material point being assessed. This unique feature makes the τ-MVM very effective from a computational point of view. Therefore, the τ-MVM is more efficient than the other existing method not only in the presence of variable amplitude load histories, but also in the presence of constant amplitude fatigue loading.

In order to understand the way the MVM works in practice, consider the component shown in Fig. 5. The algorithm proposed in Ref. [55] allows the plane containing the direction, MV, experiencing the maximum variance of the resolved shear stress to be determined. As soon as the orientation of the critical plane is known, the mean value, $\sigma_{n,m}$, and the amplitude, $\sigma_{n,a}$, of the stress normal to the critical plane, $\sigma_n(t)$, can directly be determined according to the following standard definitions [41]:

$$\sigma_{n,m} = \frac{1}{2}\left(\sigma_{n,max} + \sigma_{n,min}\right) \tag{10}$$

$$\sigma_{n,a} = \frac{1}{2}\left(\sigma_{n,max} - \sigma_{n,min}\right) \tag{11}$$

where $\sigma_{n,max}$ and $\sigma_{n,min}$ are the maximum and minimum values of $\sigma_n(t)$, respectively.

Since the direction of $\tau_{MV}(t)$ is fixed [41], the mean, τ_m, and the amplitude, τ_a, of the shear stress are also straightforward to determine, i.e.:

$$\tau_m = \frac{1}{2}\left(\tau_{MV,max} + \tau_{MV,min}\right) \tag{12}$$

$$\tau_a = \frac{1}{2}\left(\tau_{MV,max} - \tau_{MV,min}\right) \tag{13}$$

For the sake of clarity, the way the stress quantities relative to the critical plane are defined is also explained in Figs 5c and 5d graphically.

4. Proposed methodology to estimate finite lifetime under CA fretting fatigue loading

The flow-chart reported in Fig. 6 summarises the design methodology that is proposed in the present paper to use in situations of practical interest to estimate fretting fatigue lifetime. Firstly the linear-

elastic multiaxial stress distribution along the focus path has to be estimated using either numerical or analytical methods. In this context, as shown in Fig. 6, the focus path is defined as the straight line emanating from the assumed crack initiation location, A, and perpendicular to the contact surface. Secondly, calibration functions $\tau_{A,Ref}(\rho_{eff})$ and $k_\tau(\rho_{eff})$ - Eqs (2) to (6) - and the critical distance vs. number of cycles to failure law, $L_M(N_f)$ - Eq. (8), have to be determined through the parent material fatigue properties as described in Section 2.

Having calibrated functions $L_M(N_f)$, $\tau_{A,Ref}(\rho_{eff})$, and $k_\tau(\rho_{eff})$, finite lifetime under fretting fatigue can be estimated directly according to the recursive procedure summarised in Fig. 6. In particular, this procedure takes as a starting point the fact that the stress quantities relative to the critical plane – i.e., $\tau_a(r)$, $\sigma_{n,a}(r)$, $\sigma_{n,m}(r)$ – and, consequently, the critical plane stress ratio, $\rho_{eff}(r)$, can be determined, along the focus path, at any distance r from the assumed crack initiation location, A (Fig. 6). According to the τ-MVM, at any point belonging to the focus path the critical plane has to be determined by locating that material plane containing the direction experiencing the maximum variance of the resolved shear stress. For a given distance, r, from the assumed crack initiation location (Fig. 6), after calculating $\rho_{eff}(r)$ and $\tau_a(r)$ as well as the corresponding values of the MWCM's calibrating functions - i.e., $\tau_{A,Ref}(\rho_{eff})$ and $k_\tau(\rho_{eff})$, the resulting number of cycles to failure, N_f, can be predicted according to Eq. (7). As soon as N_f is known for the r value under investigation, the associated critical distance, $L_M(N_f)$, can be estimated directly via Eq. (8). Since, according to this *modus operandi*, N_f, can be estimated at any point on the focus path, the mechanical assembly being assessed is assumed to fail at the number of cycles to failure, $N_{f,e}$, as given by Eq. (9) [36].

5. Validation by experimental data

5.1. Summary of the experimental results being used

In 1988 Nowell carried out a fretting fatigue experimental investigation by using the Dartec servo-hydraulic fatigue testing machine available in the Engineering Department of the University of Oxford, UK [18]. The set-up of the experimental rig that was used by Nowell is similar to the one

shown in Fig. 1. In particular, the tests were run using a pair of cylindrical fretting pads that were pushed by a normal constant force, P, against flat-dog-bone specimens. The pads were attached to a rigid base via springs, while the specimens were clamped using a fixed and a movable jaw to enable the fatigue machine to apply to the specimens a fully-reversed sinusoidal bulk stress. The springs connecting the pads were designed to result in a fully-reversed oscillatory tangential force that was in-phase with the bulk stress applied to the specimens. The fretting pads and the specimens were made of Al/4%Cu. The relevant mechanical properties of the material being tested were as follows: σ_A=124 MPa (at $5 \cdot 10^8$ cycles to failure), E=74 GPa and σ_{UTS}=500 MPa.

Four different series of fretting fatigue trials were run by recording the number of cycles to failure resulting from any specimens being tested. In each series, unless failure occurred earlier, the fretting fatigue tests were run up to 10^7 cycles. For a given series, the peak constant pressure, P_0, the remote bulk stress and the ratio between tangential and normal load, Q/P, were kept all constant. During testing, different fretting pads were used, with these pads having radius of curvature, R_p, ranging from 12.5 mm to 150 mm. The effect of this approach was to vary the size of the contact, and hence the stress gradient in the specimen without changing the maximum stress. All tests were run in a partial slip condition, i.e., $Q<f \cdot P$, where the friction coefficient, f, was equal to 0.75. Tab. 1 summarises the relevant experimental data which will be used below to check the overall accuracy of the proposed design method.

The second set of experimental data considered in the present investigation was generated by Szolwinski et al. [6] who carried out CA fretting fatigue experiments at a frequency of 10 Hz by using an experimental set-up similar to the one sketched in Fig. 1. In more detail, the testing device consisted of two fretting pads pushed against the specimens being tested by a constant force, P. A cyclic tangential force Q was then applied in phase with a CA cyclic bulk stress. The fretting pads and the specimens were made of Al 2024-T351, i.e. an aluminium alloy having yield stress, Poisson's ratio and Young's modulus equal to 310 MPa, 0.33 and 74.1 GPa, respectively. The fretting flat-dog-bone specimens being employed had thickness equal to 12.7 mm and length equal to 330 mm. The cylindrical fretting pad had thickness equal to 12.7 mm and contact radius equal to 127 mm, 178 mm or 229 mm. Several experimental tests were conducted in partial slip conditions, i.e. $Q<f \cdot P$, and the friction coefficient, f, was estimated to be equal to 0.65. Szolwinski et al. [6] also varied the contact

force, P, in the range 5201N-7226N, the Q/P ratio in the range 0.21-0.52, and the remote bulk stress in the range 81 MPa-115.8 MPa. The load ratio characterising all the tests being run was treated as being fully-reversed (i.e., R=-1). Tab. 2 summarises the relevant experimental data that will be used below to assess the accuracy of the proposed methodology in estimating fretting fatigue lifetime.

The third set of experimental results being re-analysed in the present investigation were generated by Wittkowsky et al. [56]. The fretting pads and the specimens used in this experimental campaign were made of a 7075-T6 aluminium alloy with σ_{UTS}=572 MPa, ν=0.33 and E=72 GPa [14, 56]. The fretting pads were spherical with a radius of 25.4 mm, whereas the fretting specimens had square section of 5 mm x 5 mm. The coefficient of friction used in this experiment was 1.2. The experimental set-up used by Wittkowsky et al. [56] to generate their experimental results is again similar to that shown in Fig. 1. In more detail, during testing, two fretting pads were pushed against the specimens by a constant force P, with the fully-reversed CA cyclic tangential force, Q, being in-phase with the fully-reversed CA cyclic bulk stress. The relevant experimental data generated by Wittkowsky et al. [56] are summarised in Tab. 3.

The fourth set of validation data being considered was produced by Venkatesh et al. [57]. They performed a series of CA fretting tests run, at 10 Hz, using spherical pads and specimens made of Ti-6Al-4V. The material yield stress, ultimate tensile strength, Poisson's ratio and Young's modulus were equal to 963 MPa, 1016 MPa, 0.34 and 116 GPa, respectively. The fretting flat-dog-bone specimens had thickness equal to 12.7 mm and length to 136 mm. The fretting pads were manufactured with a contact radius equal to 12.7 mm as well as to 25.4 mm. During testing, the specimens were subjected to constant normal force P (that was generated by pushing two fretting pads against the samples themselves) as well as to a fully-reversed CA cyclic tangential force Q applied in-phase with the fully-reversed CA cyclic bulk stress, σ_b. Several fretting fatigue tests were run in a partial slip regime, i.e. $Q<f \cdot P$, where the friction coefficient, f, was equal to 0.95. A number of experimental trials were carried out by making the remote bulk stress vary in the range 225 MPa-394 MPa, the contact force in the range 22 N-70 N, and the tangential force in the range 10 N-30 N. Table 5 summarises the relevant experimental results generated by Venkatesh et al. [57] according to the experimental protocol briefly summarised above.

The last data set being considered was produced by Ferry et al. [58] by using cylindrical pads and specimens made again of Ti-6Al-4V. Three different pads having radius equal to 20 mm, 50 mm and 70 mm were employed, with the experimental set-up used to generate these results being similar to the one of Fig. 1. In more detail, two fretting pads were pushed against the specimens by a constant force, P, resulting in a peak contact pressure of 500 MPa. Further, a fully reversed CA cyclic tangential force, Q, was applied in-phase with a CA cyclic bulk stress. Al the tests were run at a frequency of 10 Hz, with the bulk stress being characterised by a load ratio, R, equal to 0. All tests were conducted under partial slip condition, i.e. $Q<f \cdot P$, with the friction coefficient, f, being equal 0.5. As to this value for f, it is interesting to observe that it is different from the one reported by Venkatesh et al. [57] for the same material. This can be ascribed to the fact that the pads used by Ferry et al. [58] were cylindrical, whereas those employed by Venkatesh et al. [57] were spherical, with this resulting in different values for the friction coefficient. Finally, run-out tests were stopped at 10^6 cycles. Tab. 5 lists the results that were generated by Ferry et al. [58] according to the experimental procedure being summarised above.

To conclude, it can be pointed out that all the experimental results being considered in the present investigation were generated by testing relatively small specimens. This resulted in the fact that, in general, the number of cycles required to initiate the fatigue cracks was larger than the number of cycles needed to propagate them until complete breakage took place. Accordingly, the experimental values of N_f that will be used in what follows to check the accuracy of the approach being proposed can be treated as the number of cycles resulting in the initiation of technical fatigue cracks, with this assumption resulting just in a little loss of accuracy.

5.2. Stress analysis

Much experimental evidence suggests that, under fretting fatigue loading, cracks tend to initiate mainly at the trailing edge of the contact zone. Therefore, the hypothesis can be formed that fretting fatigue damage can be estimated accurately by directly examining the stress fields in the vicinity of the contact. If the methodology described in Section 4 is adopted, then the linear-elastic stress distribution along the focus path defined in Fig. 6 needs to be determined either using suitable analytical solutions or by solving conventional FE contact models. Owing to the fact that the

experimental results being re-analysed in the present investigation (Section 5.1) were all generated by using standard testing configurations (see Fig. 1), the required stress fields were determined by taking full advantage of the analytical framework described in Ref. [1]. The linear-elastic stress distributions along the focus path due to the normal force, the tangential load and the remote bulk stress were computed separately for any experimental tests being considered. Subsequently, the resulting surface and sub-surface stress tensors at any point along the focus paths were obtained by simply using the superposition principle. Finally, as reviewed in Section 3, critical plane stress components $\sigma_{n,m}$, $\sigma_{n,a}$ and τ_a were determined along the focus paths by making use of the τ-MVM.

5.3 Calibration of the MWCM's governing equations

In order to use the MWCM according to the design methodology discussed in Section 4, governing equations (2) to (6) have to be calibrated via conventional fatigue results generated by testing un-notched specimens. This requires the slopes, $-1/k$ and $-1/k_0$, and the endurance limits, σ_A and τ_A, for the uniaxial and torsional fully-reversed plain fatigue curves. Unfortunately, for the materials tested in fretting, this information was not always explicitly given. Accordingly, a number of simplifying hypotheses were formed in order to calibrate the MWCM governing equations.

For the results generated using specimens of Al/4%Cu, it is reported in Ref. [18] that this material had a fully-reversed endurance limit, σ_A, extrapolated at $N_A = 5 \cdot 10^8$ cycles to failure equal to 124 MPa, with the ultimate tensile strength being equal to 500 MPa. According to the empirical rules reported in Refs [59-61], the negative inverse slope of the uniaxial fatigue curve for R=-1 was estimated as:

$$k = \frac{log(N_A/N_S)}{log(\sigma_S/\sigma_A)} \tag{13}$$

where

$$\sigma_S = 0.75 \cdot \sigma_{UTS} \text{ at } N_S = 10^3 \text{ cycles to failure} \tag{14}$$

Owing to the fact that the fully-reversed torsional fatigue curve for Al/4%Cu is not reported in Ref. [18], it was estimated as follows [59-61]:

$$\tau_A = 75 \text{ MPa at } N_A = 5 \cdot 10^8 \text{ cycles to failure} \tag{15}$$

$$k_0 = \frac{log(N_A/N_S)}{log(\tau_S/\tau_A)} \text{ with } \tau_S = 0.63 \cdot \sigma_{UTS} \text{ at } N_S = 10^3 \text{ cycles to failure} \tag{16}$$

As to the amplitude of the fully-reversed torsional endurance limit for Al/4%Cu, the reported value, Eq. (15), is the one that is recommended in Ref. [60] for aluminium alloys having a material ultimate tensile strength larger than 336 MPa and is derived from the axial endurance limit according to von Mises' criterion.

Turning to the specimens of Al 2024-T351 [6], the ultimate tensile strength for a similar material was suggested by Hojjati-Talemi et al. [21] to be equal to 506 MPa. Using this material property, the fully-reversed endurance limit, σ_A, at $N_A = 5 \cdot 10^8$ cycles to failure was estimated to be equal 130 MPa [59-61], with the associated negative inverse slope, k, being derived via Eqs (13) and (14). As with Al/4%Cu, the constants characterising the fully-reversed torsional fatigue curves were estimated directly by using Eqs (15) and (16). For aluminium alloy 7075-T6 [56], the uniaxial and torsional fully-reversed endurance limit determined at $N_A = 10^7$ cycles to failure were directly taken from Refs [62, 63]. Observing that this material had an ultimate tensile strength, σ_{UTS}, equal to 572 MPa [62], the negative inverse slopes of the uniaxial and torsional fatigue curves were estimated, for R=-1, according to Eqs (13) to (16).

Finally, the constants of the relevant plain fatigue curves for Ti-6Al-4V [57, 58] were directly taken from Ref. [64].

The values for k, k_0, σ_A, τ_A, and N_A used to calibrate the MWCM governing equations are summarised in Tab. 6. For all the materials listed in Tab. 6, the assumption was made that the mean stress sensitivity index, m, needed to determine stress ratio ρ_{eff} in Eq. (1) was equal to unity (i.e., full mean stress sensitivity). This conservative assumption was made because of the unavailability of specific experimental results suitable for determining index m.

5.4. Calibration of the L_M vs. N_f relationships

As explained in Figure 3, the calibration of the L_M vs. N_f relationship, Eq. (8), should ideally be carried out by using the fully-reversed plain fatigue curve and a fully-reversed fatigue curve generated by testing specimens containing a known geometrical feature [35]. Since, unfortunately, no notch fatigue data were reported in the original literature sources, initially the required notch fatigue curves were estimated as described in what follows.

For Al/4%Cu, Al 2024-T351 and Al 7075-T6, suitable notch endurance limits, σ_{An}, were derived by making use of Peterson's approach [65]. In particular, σ_{An} was directly estimated from the notch fatigue strength reduction factor, K_f, which is defined as [65]:

$$K_f = \frac{\sigma_A}{\sigma_{An}}, \tag{17}$$

It is important to point out here that, in definition (17), both the plain, σ_A, and the notched material high-cycle fatigue strength, σ_{An}, have to be determined at the same reference number of cycles to failure, N_A.

For the aluminium alloys under investigation, three reference values for K_f were taken from Refs [66-68]. In these papers the experimental values for the fatigue strength factors for aluminium alloys having similar characteristics/composition to the ones considered in the present study were reported explicitly. In particular, for aluminium alloy Al/4%Cu, a notch endurance limit at $2 \cdot 10^7$ cycles to failure equal to 93.4 MPa was derived from a K_f value of 1.74, with this K_f value being determined from a set of experimental results generated by testing cylindrical specimens with fillet radius, r_n, equal 0.635 mm and net stress concentration factor, K_t, equal to 1.79 [68]. For Al 2024-T351, σ_{An} at 10^7 cycles to failure was estimated to be equal to 64 MPa, with this value being determined from an experimental trial run by testing flat fillet specimens with notch radius equal to 0.5 mm (K_t=4 and K_f=2.8) [66, 67]. Finally, a notch endurance limit of 149.3 MPa (at $N_A=10^6$ cycles to failure) was estimated for Al 7075-T6 from a K_f value of 1.41 that was determined experimentally by testing cylindrical specimens with fillet radius, r_n, equal 0.635 and K_t equal to 1.79 [68].

As to the values of the notch endurance limits reported above for Al/4%Cu, Al 2024-T351, and Al 7075-T6, it is important to point out that they were estimated from the employed fatigue strength reduction factors by re-calculating, via the fatigue curves listed in Tab. 6, the corresponding plain endurance limits at the same number of cycles to failure as the one for which the different K_f values being used were given in the original sources (see Tab. 7).

After estimating σ_{An} for the three aluminium alloys of interest, the inverse negative slopes of the virtual notch fatigue curves being used to calibrate the corresponding L_M vs. N_f relationships were determined by assuming that, under fully-reversed loading, the amplitude of the notch net stress equals the material ultimate tensile stress at $N_S=10^3$ cycles to failure [60, 69]. The virtual notch fatigue curves estimated according to the assumptions discussed above are summarised in Tab. 7 in terms of notch endurance limit, σ_{An}, at N_A cycles to failure and negative inverse slope, k.

In order to employ the procedure summarised in Fig. 3 to estimate the L_M vs. N_f relationships for Al/4%Cu, Al 2024-T351 and Al 7075-T6, the required local linear-elastic stress fields were estimated by using the well-known analytical solution due to Glinka and Newport [70]. In these equations, the values for K_t and r_n were taken equal the corresponding values characterising the notch specimens used to determine the notch fatigue curves (see Table 7). This simple procedure returned the following L_M vs. N_f relationships:

$$\text{Al/4\%Cu} \Rightarrow \quad L_M = 15.2 \cdot N_f^{-0.312} \text{ [mm]} \tag{18}$$

$$\text{Al 2024-T351} \Rightarrow \quad L_M = 12.6 \cdot N_f^{-0.231} \text{ [mm]} \tag{19}$$

$$\text{Al 7075-T6} \Rightarrow \quad L_M = 21.7 \cdot N_f^{-0.347} \text{ [mm]} \tag{20}$$

For Ti-6Al-4V instead, constants A and B in Eq. (8) were directly determined from the notch results reported in Ref. [64]. In particular, Berto et al. [64] tested, under fully-reversed axial loading, V-notched cylindrical specimens of Ti-6Al-4V with r_n=0.1 mm (resulting in a K_t value of about 7.5). The notch fatigue curve determined by testing these samples is reported in Tab. 7 in terms of σ_{An} and k. Since for this set of data the relevant dimensions of the notched specimens were all available, the linear-elastic stress field in the vicinity of the notch tip was determined numerically using FE code

ANSYS®, with a simple axisymmetric model where the mesh density in the region of interest was gradually increased until convergence occurred. The obtained stress-distance curve together with the corresponding plain (Tab. 6) and notch (Tab. 7) fatigue curves were then used, as shown in Fig. 3, to determine the constants in the L_M vs. N_f relationship, obtaining:

Ti-6Al-4V $\Rightarrow$ $$L_M = 0.42 \cdot N_f^{-0.135} \text{ [mm]} \quad (21)$$

The reasoning discussed above makes it evident that constants A and B in Eq. (8) were estimated using a number of simplifying hypotheses. Although the assumptions made were based on state-of-the-art understanding and experimental data from the literature, the use of these simplifications is clearly expected to affect the overall accuracy. Therefore, with the aim of reducing the level of uncertainty, an alternative procedure was also followed to obtain more reliable values for parameters A and B in Eq. (8). These constants were determined by post-processing, for each material, a set of experimental data generated under fretting fatigue loading. This was justified since, according to the TCD, fatigue damage depends solely on profile and magnitude of the local linear-elastic stress gradients.

The procedure to determine the L_M vs. N_f relationship following this second approach is summarised in Fig. 7. According to the PM [16, 28, 29], given the value of the number of cycles to failure determined experimentally from a fretting fatigue test (i.e., $N_f = N_{f,i}$ in Fig. 7), the linear-elastic stress field determined analytically as described in Section 5.2 was used to estimate the distance, $L_M(N_{f,i})/2$, from the assumed crack initiation point (i.e., point A in Fig. 7b) at which the linear-elastic maximum principal stress, $\Delta\sigma_{1,i}$, was equal to the stress to be applied to the plain material to generate a failure at $N_{f,i}$ cycles to failure. This simple methodology allowed us to estimate the critical distance value in the medium- and in the high-cycle fatigue regime for any considered material (Fig. 7b). Finally, the least-squares method was used to interpolate the values of the characteristic lengths determined according to this simple procedure, so that constants A and B in Eq. (8) could be determined directly. The chart of Fig. 8 summarises the results that were obtained according to the methodology summarised in Fig. 7 for the materials under investigation, with the calculated values for constants A and B being also reported in this diagram.

5.5. Accuracy of the proposed fretting fatigue design methodology

For the experimental results listed in Tabs 1 to 5, the estimated, $N_{f,e}$, vs. experimental, N_f, number of cycles to failure diagrams are reported in Figs 9 and 10. The predictions were made by determining the relevant stress fields along the focus paths (Fig. 6) using the analytical method described in Ref. [1] (see Section 5.2), whereas the required plain material fatigue properties and the associated L_M vs. N_f relationships were estimated as discussed under 5.3 and under 5.4, respectively.

The error charts of Figs 9 and 10 demonstrate that the use of the proposed fretting fatigue design methodology resulted in reliable predictions, despite the assumptions that were made to derive the calibration information. By comparing the estimates shown in Fig. 9 to those reported in Fig. 10, it can be seen that, as expected, the predictions obtained by using the L_M vs. N_f relationships calibrated from fretting fatigue results (Fig. 8) resulted in a higher precision. However the predictions in Fig. 9 are remarkably accurate, with this holding true even if the notch curves used to determine the L_M vs. N_f relationships were estimated.

The agreement between experimental results and estimates shown by the charts of Figs 9 and 10 strongly supports the idea that the MWCM used in conjunction with the PM and τ-MVM is capable of capturing the main physical processes of crack initiation under CA fretting fatigue loading. In this setting, clearly, the overall accuracy of the proposed approach is expected to increase remarkably when the required calibration information is determined experimentally according to the different strategies discussed earlier. At the same time, the good level of accuracy as seen in Figs 9 and 10 suggests that the proposed fretting fatigue design methodology might be used in practical situations to perform assessment by simply estimating the necessary material fatigue properties via classical empirical equations [59-61], with this reducing the time and costs associated with the design process itself.

6. Conclusions

- According to the proposed fretting fatigue design methodology, stress gradients in the vicinity of the crack initiation locations are directly handled via the TCD, whilst the MWCM accounts for the presence of non-zero mean stress as well as for the degree of multiaxiality and the non-proportionality of the local load history.

- The MWCM applied in conjunction with the τ-MVM and the PM is seen to be capable of predicting finite lifetime of metallic materials subjected to CA fretting fatigue loading.
- Since the required stress analysis can be performed by solving conventional linear-elastic FE models, the proposed fretting fatigue assessment technique is suitable for design of real mechanical assemblies against fretting fatigue.
- Because the stress components relative to the critical plane are determined via the τ-MVM, rapid fretting fatigue lifetime estimates can be obtained independently from the complexity of the load history.
- More work needs to be done in this area to extend the use of the proposed design methodology to those situations involving variable amplitude fretting fatigue loading.

Acknowledgment

Financial support for this Industrial CASE project from EPSRC (www.epsrc.ac.uk) and Cummins Inc. (www.cummins.com) is gratefully acknowledged.

References

[1] Hills D, Nowell D. Mechanics of Fretting Fatigue. Kluwer Academic, Dordrecht, The Netherlands, 1994.

[2] Waterhouse RB. Fretting fatigue. Int Mater Rev 1992;37:77-98.

[3] Attia MH, Waterhouse RB (Editors). Standardization of fretting fatigue test methods and equipment. ASTM STP 1159, American Society of Testing and Materials, Philadelphia, PA, 1992

[4] Neu RW. Progress in standardization of fretting fatigue terminology and testing. Tribo Int 2011;44:1371–1377.

[5] Hutson AL, Nicholas T, Goodman R. Fretting fatigue of Ti-6Al-4V under flat-on-flat contact. Int J Fatigue 1999;21:663-669.

[6] Szolwinski MP, Farris TN. Observation, analysis and prediction of fretting fatigue in 2024-T351 alluminum alloy. Wear 1998;221:24-36.

[7] Rayaprolu DB, Cook R. A critical review of fretting fatigue investigations at the Royal Aerospace Establishment. In: Standardization of Fretting Fatigue Test Methods and Equipment. Edited by M. Helmi and Attia and B. Waterhouse, ASTM STP 1159, American Society for Testing and Materials, Philadelphia, USA, pp. 129-152, 1992.

[8] Hojjati-Talemi R, Wahab MA, Fretting fatigue crack initiation lifetime predictor tool: Using damage mechanics approach. Tribo Int 2013;60:176-186.

[9] Lykins C, Mall S, Jain V. An evaluation of parameters for predicting fretting fatigue crack initiation. Int J Fatigue 2000;22:703-716.

[10] Fatemi A, Socie D. A critical plane approach to multiaxial fatigue damage including out of phase loading. Fatigue Fract Engng Mat Struct 1988;11(3):149-165.

[11] Smith KN, Watson P, Topper TH. A stress strain function for fatigue of metals. ASTM Journal of Materials 1970;5:767-779.

[12] Szolwinski MP, Farris TN. Mechanics of fretting fatigue crack formation. Wear 1996;198(1–2):93-107.

[13] Ruiz C, Boddington PHB, Chen KC. An Investigation of Fatigue and Fretting in a Dovetail Joint. Exp Mech 1984;24:208–217.

[14] Navarro C, Garcia M, Dominguez J. A procedure for estimating the total life in fretting fatigue. Fatigue Fract Engng Mat Struct 2003;26(5):459-468.

[15] Nowell D, Dini D, Dyson I. The use of notch and short crack approaches to fretting fatigue threshold prediction: Theory and experimental validation. Tribo Int 2006;39:1158–1165.

[16] Taylor D. Geometrical effects in fatigue: a unifying theoretical model. Int J Fatigue 1999;21:413-420.

[17] Dini D, Nowell D, Dyson, IN. Experimental validation of a short crack approach for fretting fatigue threshold prediction. In: Proceedings of the 12th International Conference on Experimental Mechanics, Edited by C. Pappalettere, Bari, Italy, 29 August-2 September 2004.

[18] Nowell D. An analysis of fretting fatigue. DPhil Thesis, University of Oxford, Oxford, UK, 1988.

[19] Nowell D, Rajasekaran R. Fretting fatigue in dovetail blade roots: Experiment and analysis. Tribo Int 2006;39:1277-1285.

[20] Nowell D, Araújo JA. Analysis of pad size effects in fretting fatigue using short crack arrest methodologies. Int J Fatigue 1999;21:947-956.

[21] Hojjati-Talemi R, Wahab A, Pauw J, Baets P. Prediction of fretting fatigue crack initiation and propagation lifetime for cylindrical contact configuration. Tribo Int 2014;76:73-91.

[22] Noraphaiphipaksa L, Manonukul A, Kanchanomai C. Fretting Fatigue with Cylindrical-On-Flat Contact: Crack Nucleation, Crack Path and Fatigue Life. Materials (Basel) 2017;10(2)-155;1-21.

[23] Suresh S. Fatigue of materials. Cambridge University Press, Cambridge, UK, 1998.

[24] Erdogan G, Sih G. On the crack extension in plates under plane loading and transverse shear. J Basic Eng 1963;85(4):519-525.

[25] Araújo JA, Susmel L, Pires MTS, Castro FC. A multiaxial stress-based critical distance methodology to estimate fretting fatigue life. Tribo Int 2017;108:2-6.

[26] Araújo JA, Susmel L, Taylor D, Ferro JCT, Mamiya EN. On the use of the Theory of Critical Distances and the Modified Wöhler Curve Method to estimate fretting fatigue strength of cylindrical contacts. Int J Fatigue 2007;29:95-107.

[27] Araújo JA, Susmel L, Taylor D, Ferro JCT, Ferreira JLA. On the prediction of High-Cycle Fretting Strength: Theory of Critical Distances vs. Hot spot Approach. Eng Frac Mech 2008;75:1763-1778.

[28] Susmel L. Multiaxial Notch Fatigue: from nominal to local stress-strain quantities. Woodhead & CRC, Cambridge, UK, 2009.

[29] Taylor D. The Theory of Critical Distances: a new perspective in Fracture Mechanics. Elsevier, Oxford, UK, 2007.

[30] Mamiya EN, Araújo JA. Fatigue limit under multiaxial loadings: on the definition of the equivalent shear stress. Mech Res Commun 2000;29:141-151.

[31] Araújo JA, Dantas AP, Castro FC, Mamiya EN, Ferreira JLA. On the characterization of the critical plane with a simple and fast alternative measure of the shear stress amplitude in multiaxial fatigue. Int J Fatigue 2011;33:1092–1100.

[32] Araújo JA, Carpinteri A, Ronchei C, Spagnoli A, Vantadori S. An alternative definition of the shear stress amplitude based on the maximum rectangular hull method and application to the C-S (Carpinteri-Spagnoli) criterion. Fatigue Fract Engng Mater Struct 2014;37:764-771.

[33] Carpinteri A, Ronchei C, Spagnoli A, Vantadori S. On the use of the Prismatic Hull method in a critical plane-based multiaxial fatigue criterion. Int J Fatigue 2014;68:159-167.

[34] Giannakopoulos AE, Lindley TC, Suresh S. Similarities of stress concentration in contact at round punches and fatigue at notches: implication to fretting fatigue crack initiation. Fatigue Fract Engng Mat Struct 2000;23:561-571.

[35] Susmel L, Taylor D. A novel formulation of the Theory of Critical Distances to estimate lifetime of notched components in the medium-cycle fatigue regime. Fatigue Fract Engng Mater Struct 2007;30:567-581.

[36] Susmel L, Taylor D. The Modified Wöhler Curve Method applied along with the Theory of Critical Distances to estimate finite life of notched components subjected to complex multiaxial loading paths. Fatigue Fract Engng Mater Struct 2008;31:1047-1064.

[37] Susmel L, Taylor D, Tovo R. On the estimation of notch fatigue limits by using the Theory of Critical Distances L, a_0 and open notches. Structural Durability and Health Monitoring 2008;4(1):1-18.

[38] Susmel L, Taylor D. A critical distance/plane method to estimate finite life of notched components under variable amplitude uniaxial/multiaxial fatigue loading. Int J Fatigue 2012;38:7-24.

[39] Susmel L, Taylor D. The Theory of Critical Distances to estimate lifetime of notched components subjected to variable amplitude uniaxial fatigue loading. Int J Fatigue 2011;33:900-911.

[40] Louks R, Gerin B, Draper J, Askes H, Susmel L. On the multiaxial fatigue assessment of complex three-dimensional stress concentrators. Int J Fatigue 2014;63:2014.

[41] Susmel L. Four stress analysis strategies to use the Modified Wöhler Curve Method to perform the fatigue assessment of weldments subjected to constant and variable amplitude multiaxial fatigue loading. Int J Fatigue 2014;67;38-54.

[42] Susmel L, Lazzarin P. A Bi-parametric Modified Wöhler Curve for high cycle multiaxial fatigue assessment. Fatigue Fract Eng Mater Struct 2002;25:63-78.

[43] Susmel L, Tovo R, Benasciutti D. A novel engineering method based on the critical plane concept to estimate lifetime of weldments subjected to variable amplitude multiaxial fatigue loading. Fatigue Fract Eng Mater Struct 2009; 32:441-459.

[44] Kanazawa K, Miller KJ, Brown MW. Low-cycle fatigue under out-of-phase loading conditions. J Eng Mater Technol 1977;99:222-228.

[45] Socie DF. Multiaxial fatigue damage models. J Eng Mater Technol 1987;109:293-298.

[46] Susmel L. Multiaxial fatigue limits and material sensitivity to non-zero mean stresses normal to critical planes. Fatigue Fract Eng Mater Struct 2008;31(3-4):295-309.

[47] Kaufman RP, Topper T. The influence of static mean stresses applied normal to the maximum shear planes in multiaxial fatigue. In: Biaxial and multiaxial fatigue and fracture, Edited by A. Carpinteri, M. de Freitas and A. Spagnoli, Oxford, Elsevier and ESIS, pp. 123-143, 2003.

[48] Lazzarin P, Susmel L. A stress-based method method to predict lifetime under multiaxial fatigue loadings. Fatigue Fract Eng Mater Struct 2003; 26:1171-1187.

[49] Susmel L, Tovo R, Lazzarin P. The mean stress effect on the high-cycle fatigue strength from a multiaxial point of view. Int J Fatigue 2005;27:928-43.

[50] Susmel L, Atzori B, Meneghetti G, Taylor D. Notch and Mean Stress Effect in Fatigue as Phenomena of Elasto-Plastic Inherent Multiaxiality. Eng Fract Mech 2011;78(8):2011.

[51] Susmel L, Tovo R. Estimating fatigue damage under variable amplitude multiaxial fatigue loading. Fatigue Fract Eng Mater Struct 2011;34(12):1053-1077.

[52] Bagni C, Askes H, Susmel L. Gradient elasticity: a transformative stress analysis tool to design notched components against uniaxial/multiaxial high-cycle fatigue. Fatigue Fract Eng Mater Struct 2016;39(8):1012–1029.

[53] Peterson RE. Stress concentration factors. John Wiley & Sons, New York, USA, 1974.

[54] Tanaka K. Engineering formulae for fatigue strength reduction due to crack-like notches. Int J Fracture 1983;22:R39-R45.

[55] Susmel L. A simple and efficient numerical algorithm to determine the orientation of the critical plane in multiaxial fatigue problems. Int J Fatigue 2010;32:1875-1883.

[56] Wittkowsky BU, Birtch PR, Dominguez J, Suresh S. An experimental investigation of fretting fatigue with spherical contact in 7075-T6 aluminum alloy. In: Fretting fatigue: current technology and practices, Edited by Hoeppner DW, Chandrasekaran V, Elliott CB.ASTM STP 1367, West Conshohocken, pp. 213-27, 2000.

[57] Venkatesh T, Conner B, Giannakopoulos A, Lee C, Lindley T, Suresh S, An Experimental investigation of Fretting Fatigue in Ti-6Al-4V: the Role of Contact Conditions and Microstructure. Metall and Mat Trans A 2001;32(5):1131–1146.

[58] Ferry B, Araújo J, Pommier S, Demmou K. Life of a Ti-6AI-4V alloy under fretting fatigue: Study of new nonlocal parameters. Tribo Int 2017;108:23-31.

[59] Juvinall RC, Marshek KM. Fundamentals of Machine Component Design. John Wiley & Sons, New York, USA, 1991.

[60] Lee Y-L, Pan J, Hathaway, RB, Barkey ME. Fatigue Testing and Analysis. Elsevier Butterworth–Heinemann, Oxford, UK, 2005.

[61] Susmel L. On the estimation of the material fatigue properties required to perform the multiaxial fatigue assessment. Fatigue Fract Eng Mater Struct 2013;36:565-585.

[62] Hojjati-Talemi R, Wahab MA, Giner E, Sabsabi M. Numerical Estimation of Fretting Fatigue Lifetime Using Damage and Fracture mechanics. Tribol Lett 2013;52:11–25.

[63] Sabsabi M, Giner E, Fuenmayor FJ. Experimental fatigue testing of a fretting complete contact and numerical life correlation using X-FEM. Int J Fatigue 2011;33(6):811–822.

[64] Berto F, Campagnolo A, Lazzarin P. Fatigue strength of severely notched specimens made of Ti–6Al–4V under multiaxial loading. Fatigue Fract Eng Mater Struct 2015;38(5):503–517.

[65] Peterson RE. Notch Sensitivity. In: Metal Fatigue, Edited by G. Sines and J. L. Waisman, McGraw Hill, New York, pp. 293-306, 1959.

[66] Grover HJ, Bishop SM, Jackson LR. Axial-load fatigue tests on notched sheet specimens of 24S-T3 and 75S-T6 aluminium alloys and of SAE 4130 steel with stress-concentration. National Advisory Committee for Aeronautic (NACA), Washington, Technical Note 2389, 1951.

[67] Whaley RE. Fatigue and static strength of notched and unnotched aluminum-alloy and steel Specimens. Experimental Mechanics 1962;2(11):329–334.

[68] Bennett JA, Weinberg JG. Fatigue notch sensitivity of some aluminum alloys. Journal of Research of the National Bureau of Standards 1954;52(5);235-245 (Research Paper 2495)

[69] Juvinall, R. C. and Marshek, K. M. Fundamentals of Machine Component Design. John Wiley & Sons, New York, USA, 1991.

[70] Glinka G, Newport A. Universal features of elastic notch-tip stress fields. Int J Fatigue 1987;9(3):143-150.

List of Captions

Tables

Series	P_o *[MPa]*	Q_{max}/P	$\sigma_{B,max}$ *[MPa]*	R_p *[mm]*	a *[mm]*	N_f *[Cycles]*
1	157	0.45	92.7	12.5	0.1	10^7
				25	0.19	10^7
				37.5	0.28	10^7
				50	0.38	1290000
				75	0.57	670000
				100	0.76	850000
				125	0.95	730000
				150	1.14	670000
2	143	0.45	92.7	12.5	0.09	10^7
				25	0.18	10^7
				37.5	0.27	4040000
				50	0.36	1500000
				75	0.54	800000
				100	0.72	610000
				125	0.9	1240000
				150	1.08	690000
3	143	0.45	77.2	12.5	0.09	10^7
				25	0.18	10^7
				50	0.36	10^7
				75	0.54	1200000
				100	0.72	1420000
				125	0.9	1020000
4	120	0.45	61.8	25	0.14	10^7
				37.5	0.21	10^7
				50	0.28	10^7
				75	0.42	10^7
				100	0.57	10^7
				125	0.71	1570000
				150	0.85	1230000

Table 1. Summary of the experimental results generated by Nowell by testing specimens of Al/4%Cu (run outs at 10^7 cycles to failure) [18].

R_p *[mm]*	P *[N]*	P_o *[MPa]*	Q/F	$\sigma_{b,a}$ *[MPa]*	a *[mm]*	N_f *[Cycles]*
121	4880	202.7	0.35	100.7	1.21	241016
	6316	230.6	0.31	110.3	1.37	217061
127	7562	246.0	0.22	110.3	1.54	314000
	4893	197.8	0.28	84.7	1.24	422000
	5427	208.4	0.31	110.3	1.31	241475
	6228	223.2	0.23	84.8	1.40	668277
	5370	207.3	0.35	88.4	1.30	563946
	7226	240.4	0.31	101.9	1.51	545489
	5201	204.0	0.52	115.8	1.28	465000
	6215	223.0	0.35	109.2	1.40	302804
	7070	237.8	0.27	108.8	1.49	253883
	6275	224.0	0.36	98.2	1.40	464166
	5462	209.0	0.33	97.1	1.31	311516
	7118	238.6	0.27	85.4	1.50	381535
178	6268	189.2	0.27	100.0	1.66	349520
	5310	174.2	0.38	85.8	1.53	582922
	6994	199.9	0.34	113.1	1.75	455759
	7085	201.2	0.21	85.2	1.77	665073
	7251	203.6	0.31	99.4	1.79	552250
	6176	187.9	0.27	84.7	1.65	621442
	5319	174.3	0.36	97.4	1.53	459882
	6460	192.1	0.34	106.4	1.69	225535
	5351	174.9	0.38	110.6	1.53	330695
229	5454	155.7	0.38	111.7	1.76	238000
	5427	155.3	0.37	112.9	1.75	249574
	6223	166.3	0.32	97.0	1.88	739250
	6268	166.9	0.32	85.4	1.88	856524
	7072	177.3	0.24	81.8	2.00	747135
	7073	177.3	0.25	81.8	2.00	729715
	5293	153.4	0.31	81.0	1.73	867330
	5325	153.8	0.26	82.9	1.74	768364
	7002	176.4	0.34	109.5	1.99	320864
	6187	165.8	0.33	110.8	1.87	479540
	7153	178.3	0.24	97.9	2.01	463324

Table 2. Summary of the experimental results generated by Szolwinski et al. by testing specimens of Al 2024-T351 [6].

R_p [mm]	P [N]	Q [N]	Q/F	$\sigma_{b,a}$ [MPa]	P_o [MPa]	N_f [Cycles]	Spec. status
	13.0	7.0	0.538	83.0	183	10000000	Run out
	7.3	6.6	0.904	83.0	151	3450000	Run out
	20.0	16.0	0.800	62.5	211	2190000	Run out
	20.0	15.0	0.750	56.0	211	1540000	Run out
	20.0	15.0	0.750	63.0	211	2940000	Run out
	20.0	15.0	0.750	59.0	211	1780000	Run out
	20.0	15.0	0.750	84.2	211	549000	Failure
25.4	10.3	7.5	0.728	83.6	171	2940000	Failure
	30.0	15.0	0.500	85.0	241	480000	Failure
	20.8	15.0	0.721	83.0	214	449000	Failure
	15.6	15.0	0.962	85.0	194	395000	Failure
	18.5	13.6	0.735	77.0	206	551000	Failure
	16.0	11.7	0.731	83.0	196	530000	Failure
	13.9	10.0	0.719	83.0	187	803000	Failure
	20.0	15.0	0.750	70.0	211	516000	Failure

Table 3. Summary of the experimental results generated by Wittkowsky et al. by testing specimens of Al 7075-T6 [56].

R_p [mm]	F [N]	Q [kN]	Q/F	$\sigma_{b,a}$ [MPa]	N_f [Cycles]
12.7	50	14.5	0.29	394	107899
	50	14.5	0.29	300	474656
	50	15.0	0.30	341	266176
	50	30.0	0.60	300	142746
	50	33.0	0.66	225	691612
	50	30.0	0.60	315	117183
	50	23.0	0.46	300	307653
	50	30.0	0.60	250	278238
	40	16.0	0.40	300	401153
25.4	50	15.0	0.30	341	192000
	50	15.0	0.30	325	872863
	50	32.0	0.64	300	207258
	50	21.0	0.42	300	598191
	50	30.0	0.60	375	85957
	50	30.0	0.60	320	212491

Table 4. Summary of the experimental results generated by Venkatesh et al. by testing specimens of Ti-6Al-4V [57].

R_p *[mm]*	P_o *[Mpa]*	$\sigma_{b,a}$ *[Mpa]*	Q/f·P	N_f *[Cycles]*	Spec. Status
20	500	340	0.47	225780	Failure
		320	0.47	488632	Failure
		320	0.47	477861	Failure
		310	0.47	1000000	Run out
50	500	300	0.46	164690	Failure
		300	0.46	168472	Failure
		300	0.46	189447	Failure
		300	0.46	203759	Failure
		200	0.44	541220	Failure
		200	0.44	548,69	Failure
		160	0.49	1000000	Run out
70	500	300	0.46	166150	Failure
		300	0.46	168266	Failure
		200	0.42	195225	Failure
		180	0.47	1000000	Run out

Table 5. Summary of the experimental results generated by Ferry et al. by testing specimens of Ti-6Al-4V [58].

Material	Ref.	σ_{UTS} *[MPa]*	σ_A *[MPa]*	k	τ_A *[MPa]*	k_o	N_A *[Cycles]*
Al/4%Cu	[18]	500	124.0	11.9	75.0	9.1	$5 \cdot 10^8$
Al 2024-T351	[6, 21]	506	130.0	12.2	75.0	9.1	$5 \cdot 10^8$
Al 7075-T6	[56, 62, 63]	572	166.0	9.7	95.8	7.0	10^7
Ti-6Al-4V	[57, 58, 64]	978	475.7	9.3	388.3	22.1	$2 \cdot 10^6$

Table 6. Adopted values for the constants of the plain fatigue curves used to calibrate the MWCM.

Material	r_n *[mm]*	K_t	σ_{An} *[MPa]*	k	N_A *[Cycles]*
Al/4%Cu	0.635	1.79	93.4	5.9	$2 \cdot 10^7$
Al 2024-T351	0.5	4.0	64.0	4.5	10^7
Al 7075-T6	0.635	1.79	117.7	5.1	10^6
Ti-6Al-4V [64]	0.1	7.5	100.9	6.3	$2 \cdot 10^6$

Table 7. Adopted values for the constants of the virtual notch fatigue curves used to calibrate the L_M vs. N_f relationship.

Figures

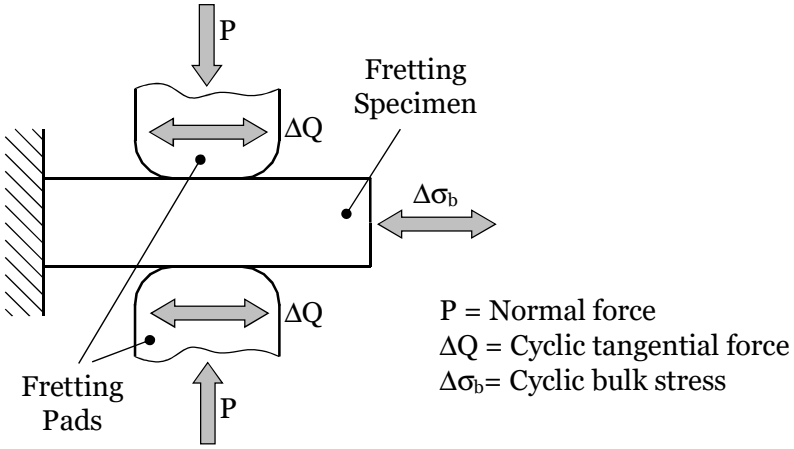

Figure 1. Typical experimental set-up of a fretting fatigue test.

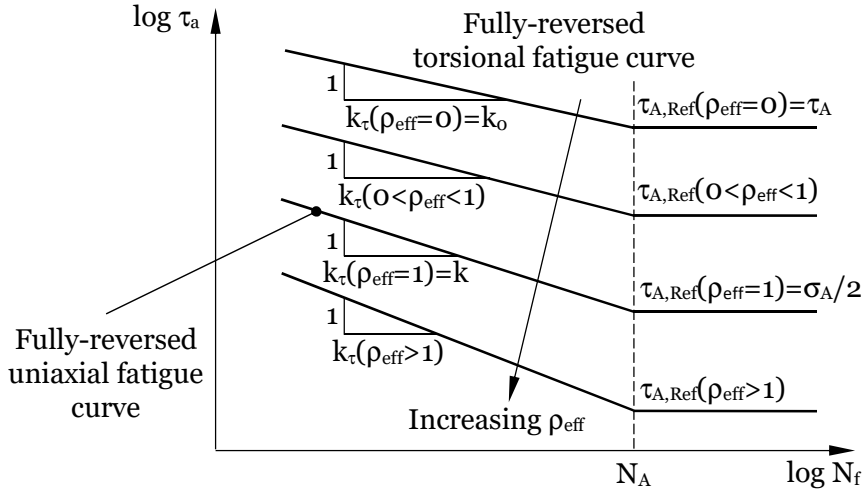

Figure 2. Modified Wöhler diagram.

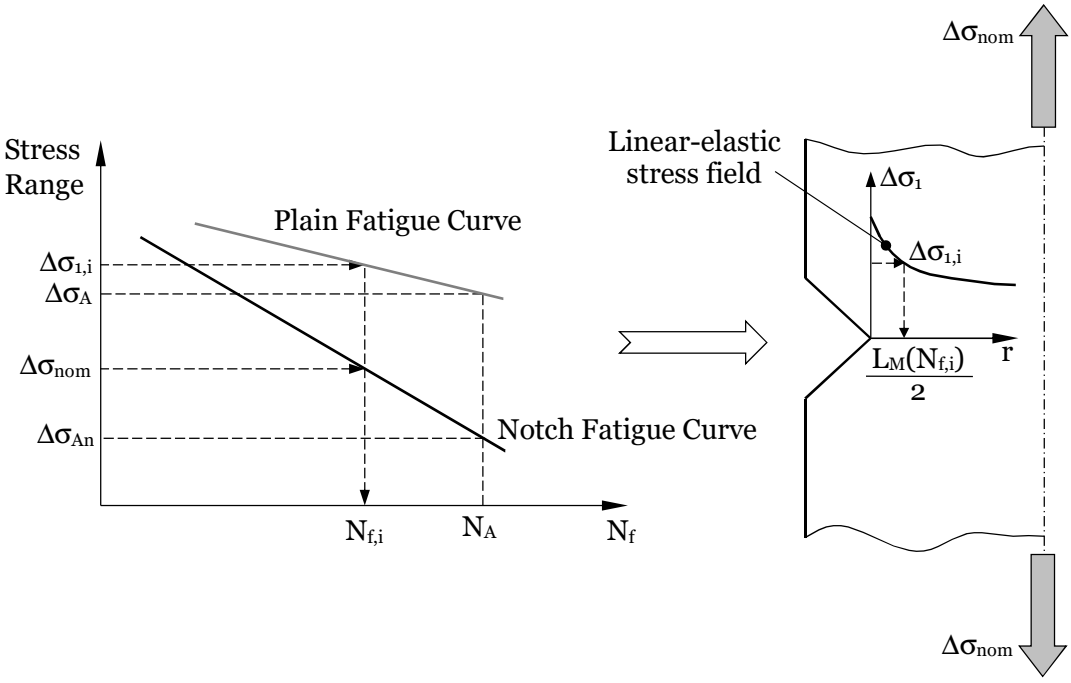

Figure 3. Procedure to determine the critical distance value in the medium-cycle fatigue regime by using two calibration fatigue curves.

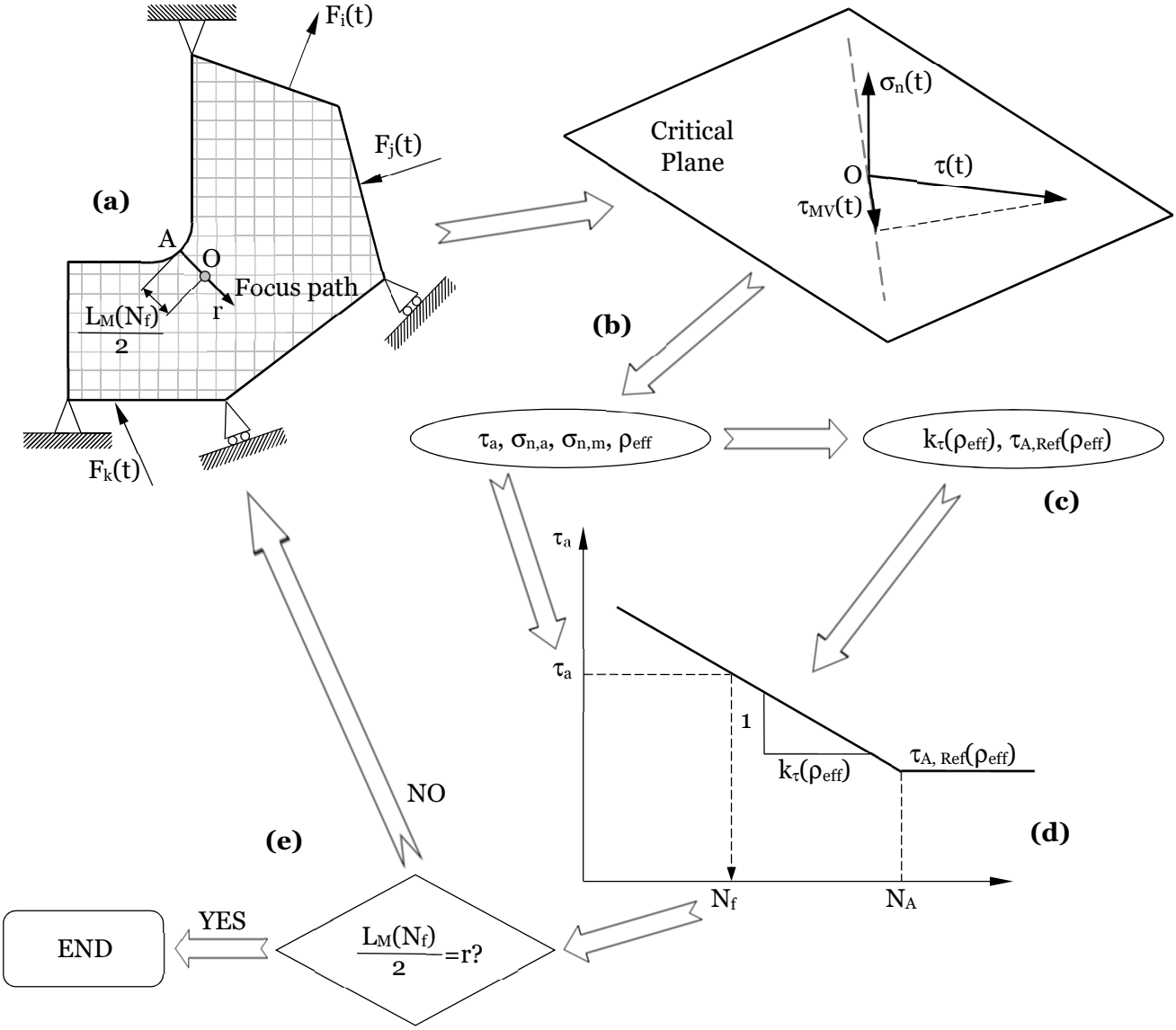

Figure 4. MWCM applied along with the PM to estimate finite lifetime of notched components subjected to in-service fatigue loading.

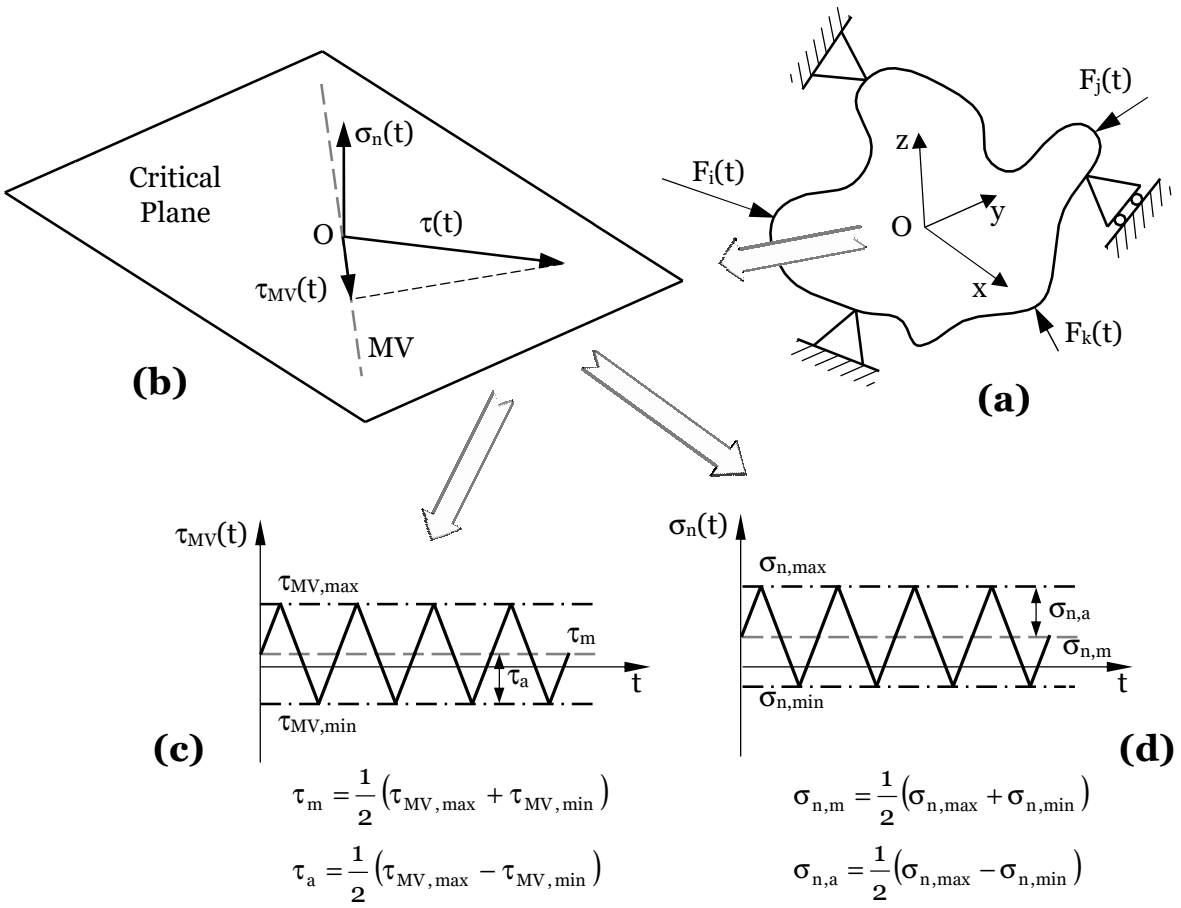

$$\tau_m = \frac{1}{2}\left(\tau_{MV,max} + \tau_{MV,min}\right) \qquad \sigma_{n,m} = \frac{1}{2}\left(\sigma_{n,max} + \sigma_{n,min}\right)$$

$$\tau_a = \frac{1}{2}\left(\tau_{MV,max} - \tau_{MV,min}\right) \qquad \sigma_{n,a} = \frac{1}{2}\left(\sigma_{n,max} - \sigma_{n,min}\right)$$

Figure 5. Amplitude and mean value of the stress components relative to the critical plane determined according to the τ-MVM.

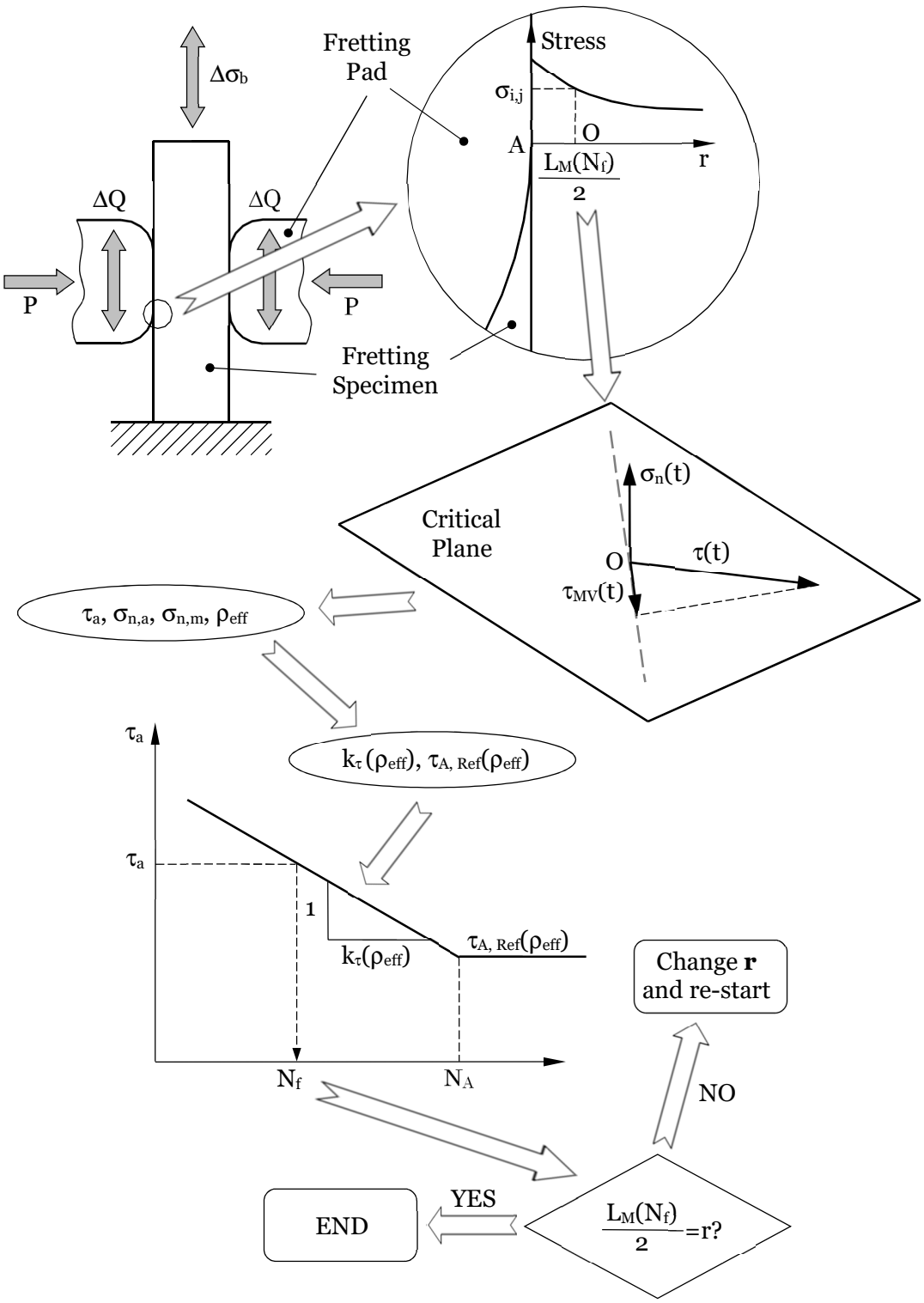

Figure 6. In-field use of the MWCM applied in conjunction with the PM to estimate finite lifetime under fretting fatigue loading.

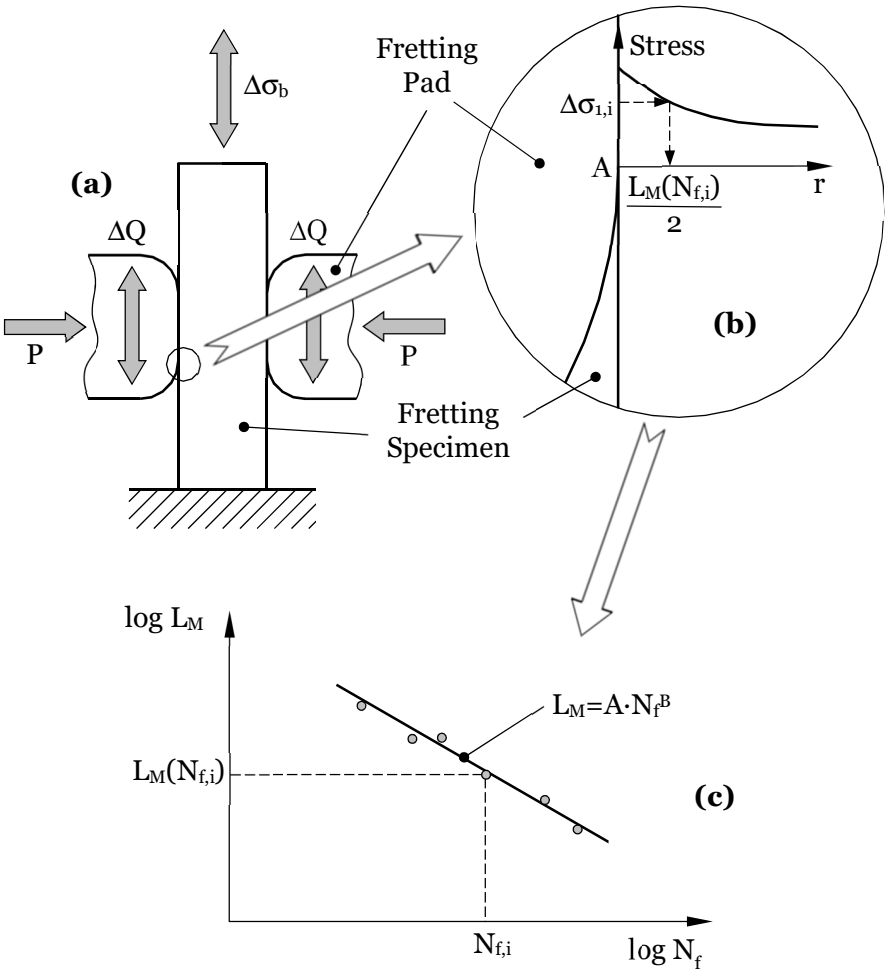

Figure 7. Determination of the L_M vs. N_f relationship by post-processing experimental results generated under fretting fatigue loading.

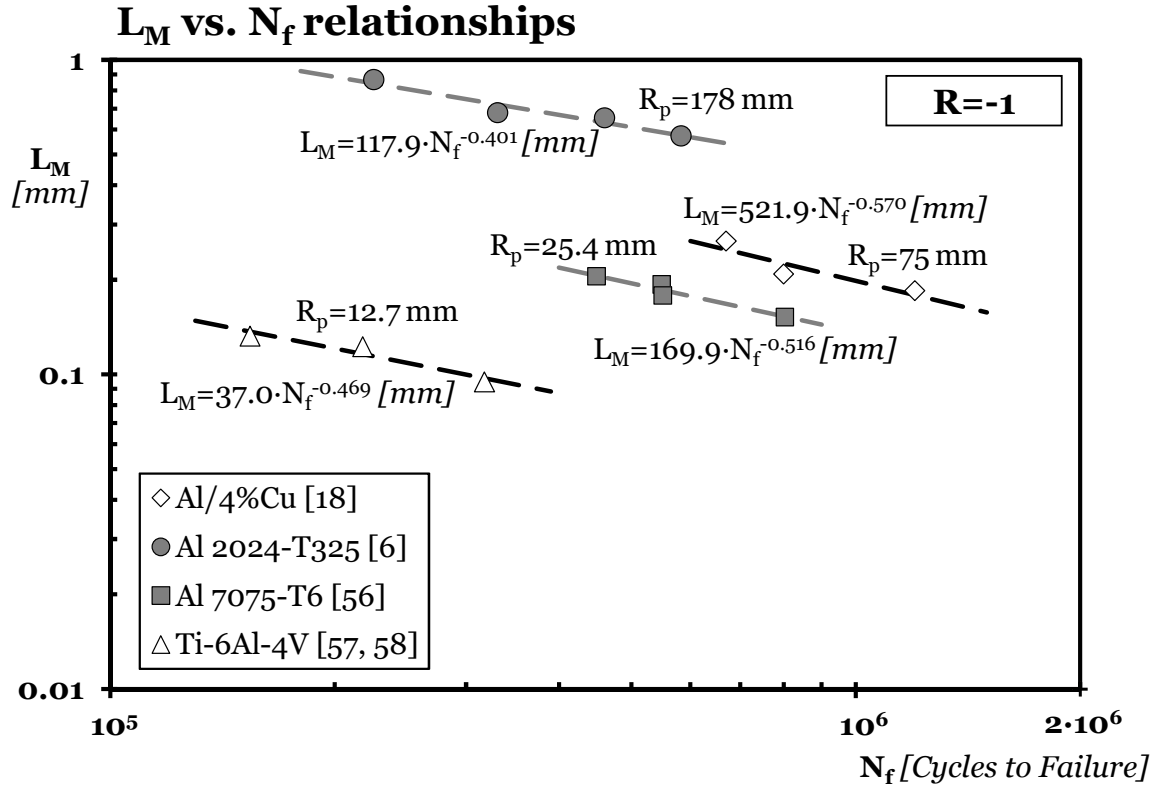

Figure 8. Calibration of the L_M vs. N_f relationships for the different materials considered in the present investigation using fretting fatigue results.

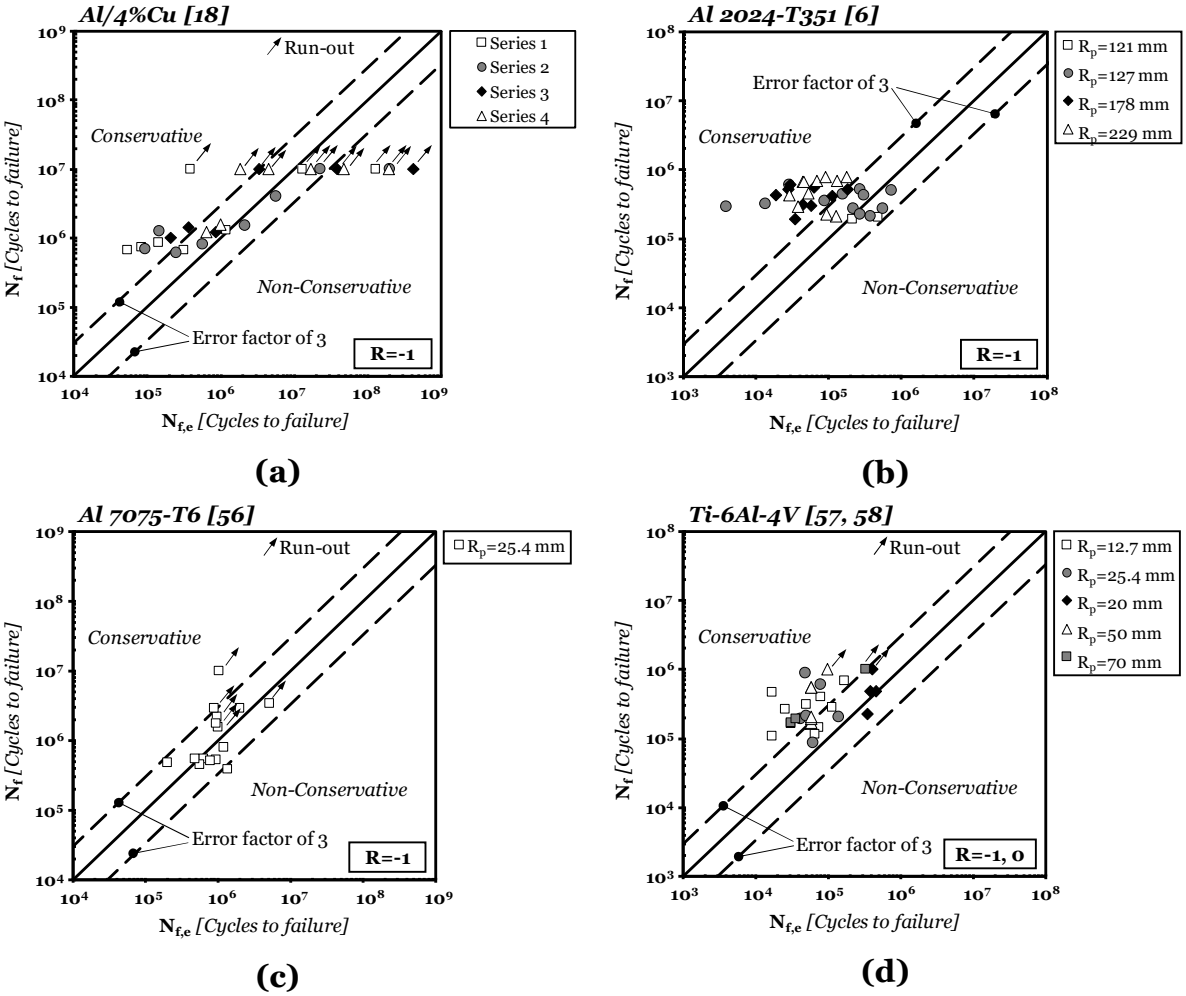

Figure 9. Accuracy of the MWCM applied along with the PM and τ-MVM in estimating fretting fatigue lifetime when the L_M vs. N_f relationships are calibrated from notch fatigue curves estimated by using K_f.

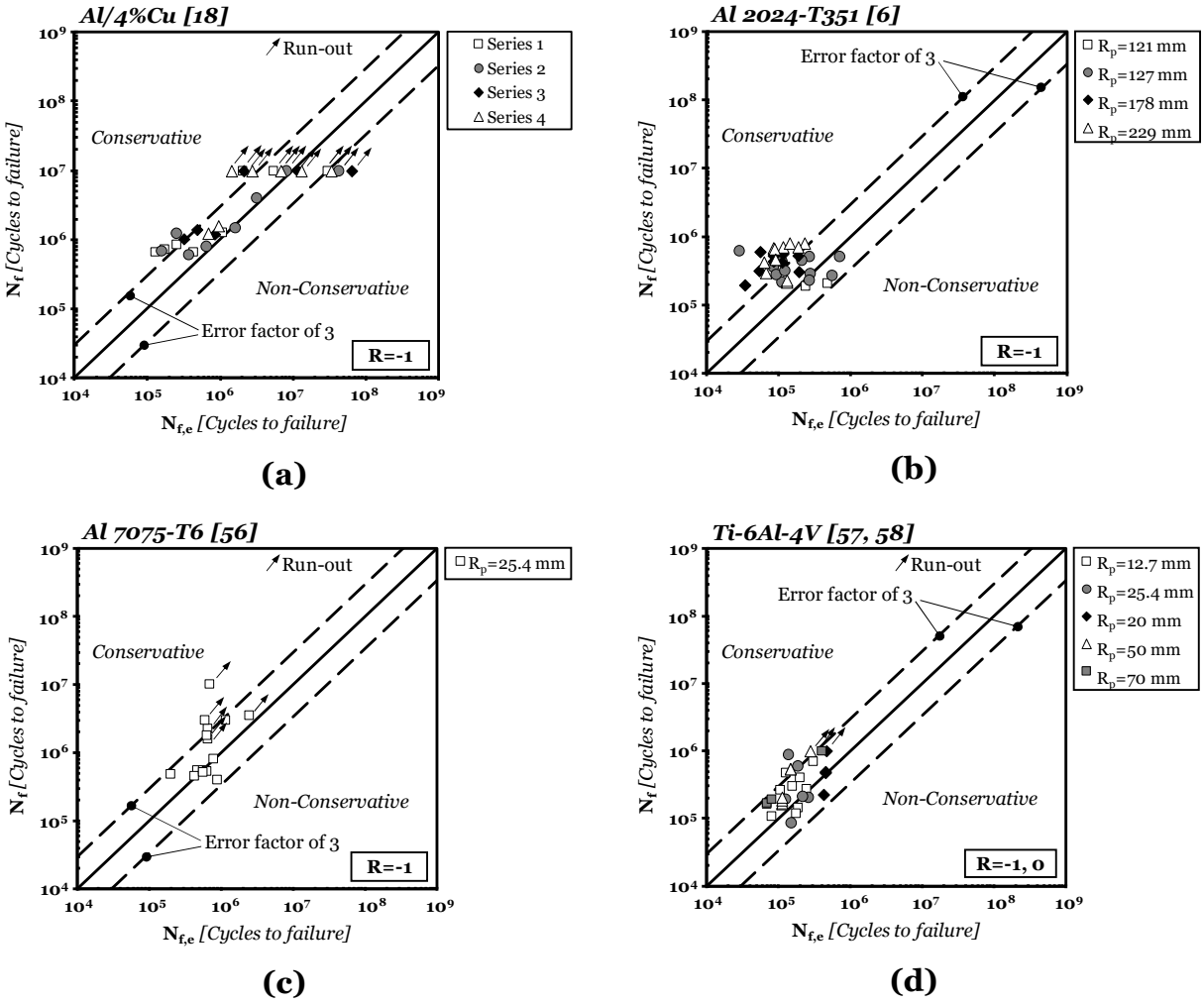

Figure 10. Accuracy of the MWCM applied along with the PM and τ-MVM in estimating fretting fatigue lifetime when the L_M vs. N_f relationships are calibrated from fretting fatigue results (see also Figure 8).